Fuel 320 (2022) 123952

Contents lists available at ScienceDirect

Fuel

journal homepage: www.elsevier.com/locate/fuel

Full Length Article

Spray and engine performance of cerium oxide nanopowder and carbon nanotubes modified alternative fuel

Zhichao Zhang [a], Yiji Lu [b,*], Zi Qian [a], Anthony Paul Roskilly [c]

[a] Department of Mechanical and Construction Engineering, Northumbria University, Newcastle NE1 8ST, United Kingdom
[b] James Watt School of Engineering, University of Glasgow, Glasgow G12 8QQ, United Kingdom
[c] Durham Energy Institute, Durham University, Durham DH1 3LE, United Kingdom

ARTICLE INFO

Keywords:
Alternative/cleaner fuel
Cerium oxide nanopowder
Carbon nanotube
Spray
Emission analysis
Internal combustion engine

ABSTRACT

This work aims to experimentally investigate and demonstrate the impacts of using Cerium Oxide (CeO_2) and multi-wall carbon nanotube (CNT) blended with the alternative fuel, which is gas-to-liquid fuel (GTL) in this study, compared to diesel fuel (DF) on engine performance and study the macroscopic spray characteristics through a Constant Volume Vessel (CVV). Results demonstrate Cerium Oxide nanopowder and carbon nanotubes have very limited impacts on the average cone angle of gas-to-liquid fuel and diesel fuel. Cerium Oxide nanopowder and carbon nanotubes can individually reduce spray penetration during injection under a small ambient pressure when blended with diesel fuel, whilst the effect on gas-to-liquid fuel is less significant because the smaller density and lighter compositions of gas-to-liquid fuel promote its breakup process. In the post-injection period, carbon nanotubes increases the spray penetration of gas-to-liquid fuel, because gas-to-liquid fuel molecules are smaller than diesel fuel. Consequently, more gas-to-liquid fuel molecules stay inside the carbon nanotubes, which can only evaporate through two ends, and thus results in an overall reduced evaporation rate. Moreover, experiments also demonstrate that the average cone angle is independent of rail pressure, but it can be reduced by decreasing ambient pressure and increasing ambient temperature. During injection, both ambient pressure and rail pressure can influence the spray penetration, whilst after the end of injection, only ambient temperature has an effect on it. The engine experiment indicates that Cerium Oxide nanopowder can reduce nitrogen oxides, unburnt hydrocarbons and particulate number emissions simultaneously for both diesel fuel and gas-to-liquid fuel due to its catalysis at high-temperature conditions, whilst carbon nanotubes has a weaker effect on reducing nitrogen oxides and particulate number for gas-to-liquid fuel than diesel fuel.

1. Introduction

Given the growing concerns about the pollutants emitted by burning fossil fuels, increasingly strict regulations have been released to restrain toxic gases and particulate matter (PM) from vehicle engines [1,2]. Research on alternative/cleaner fuels and modified fuels have been become increasingly popular, as they are likely to improve engine performance or reduce emissions. When developing and introducing a new fuel with different properties, it is essential to investigate the spray features prior to the engine test. It is because the spray is a process that liquid fuel is injected into the air, breaks out into droplets and evaporates, and this has a significant impact on the in-cylinder combustion, especially on pollutant formation [3,4].

The gas-to-liquid fuel (GTL) is one alternative/cleaner fuel derived from methane through the Fischer-Tropsch synthetic process [5,6]. It has been demonstrated to have higher cetane number (CN), ultralow aromatics content, zero sulphur content, smaller density, higher lower heating value (LHV), higher flash point, and closed viscosity compared with diesel fuel [7–9]. When implementing GTL in diesel engines, some researchers found it to produce less unburnt hydrocarbons (HC), PM and nitrogen oxides (NO_x) emissions as well as higher brake thermal efficiency [7,10] than diesel fuel. However, other studies showed that carbon monoxide (CO) and HC emissions are usually higher than standard diesel fuel (DF) and FAME-based biofuels [11,12]. In terms of spray characteristics, Kannaiyan *et al.* [13] conducted experiments in a spray chamber and noticed that the smaller viscosity and surface tension of GTL led to faster disintegration and dispersion of droplets than conventional fuel. Nevertheless, the spray experiment was conducted under

* Corresponding author.
E-mail address: yiji.lu@glasgow.ac.uk (Y. Lu).

https://doi.org/10.1016/j.fuel.2022.123952
Received 19 January 2022; Received in revised form 10 March 2022; Accepted 20 March 2022
Available online 30 March 2022

Table 1
Specifications of nano additives.

Name	Bulk density (g/cm^3)	Size (nm)	Specific surface area (m^2/g)	Bulk thermal conductivity (W/kg/K)
CNT	0.22	40 ~ 60 (diameter) 2000 (length)	Min 110	15 ~ 25
Ce25	0.53	Max 25	30 ~ 50	18.35

The thermal conductivity of CNT and Ce25 are from [25,26]. Other data is provided by the sellers.

atmospheric conditions, which is very different to conditions in engine cylinders.

Nanomaterials can be used as additives to modify fuel properties, and are expected to contribute to more output power, higher thermal efficiency, less generated pollutants [14,15]. Cerium Oxide (CeO_2) nanopowder is a metallic oxide additive, which has the potential to reduce the CO and HC emissions for all fuels because it can absorb and release free oxygen atoms via reversible reactions at high-temperature conditions, and thus provides more oxygen for the fuel at the fuel-rich zones to promote engine combustion [16,17]. Researchers have investigated its engine performance and demonstrated that NO_x and HC were reduced whilst the thermal efficiency was improved [18–20]. However, the influence of CeO_2 nano additive on spray characteristics and engine performance of GTL have yet to be studied.

Carbon nanotubes (CNT) is another nanomaterial sometimes blended with other additives in diesel fuel as an additive enhancer [21–23]. Several researchers claimed that CNT can accelerate combustion and improve efficiency and reduce pollutants such as CO and HC for diesel engines when blended with metallic oxide nanopowder [21,24]. Furthermore, some other researchers believed CNT can not only promote fast combustion reactions but also improve the fuel–air mixing for more complete combustion [15]. However, most of the studies used CNT as an enhancer to promote the dispersion of another main additive instead of a single component additive directly contributing to the combustion of fuels. As a result, the performance of CNT alone in diesel engines and its impact on fuel properties are still unclear, and therefore spray experiments and engine experiments are required in order to achieve further understanding.

In summary, GTL is a promising alternative/cleaner fuel, but its spray characteristics were not comprehensively studied at conditions close to the engine cylinder, and blending new GTL-based fuels with nano additives have the potential to further reduce the emissions. Meanwhile, most experiments on fuel spray did not consider the influence of engine conditions including fuel pressure, ambient pressure and ambient temperature. Moreover, CeO_2 nanopowder and CNT are two types of nano additives with the potential for reducing pollutant emissions and improving engine output. However, their influences on spray characteristics and engine performance of GTL have not been studied. Therefore, this work employs CeO_2 nanopowder and CNT as two single-component nano additives and investigates their blends with GTL and the diesel fuel (DF) respectively on the macroscopic spray characteristics at high ambient temperature and variable ambient pressure and engine performance. In addition, the influence of experimental conditions on spray is also analysed through experiments on DF.

2. Apparatus and methodologies

2.1. Fuel formulation

The additives to modified fuels are the multi-wall CNT which has a diameter of 40 ~ 60 nm and the length of 2 μm, and CeO_2 nanopowder with a maximum size of 25 nm (Ce25). Table 1 shows the specifications of the nanopowder additives. The CNT is provided by Shenzhen Nanotech Port Ltd, and the Ce25 is bought on Sigma-Aldrich.com.

The CNT and Ce25 are added to diesel fuel EN590 (DF) and GTL with 40 ppm concentration respectively. Both fuels are provided by Coryton Advanced Fuels Ltd,. The blends are later vibrated using a Fisherbrand 15060 ultrasonic vibrator for two hours and eventually become stable and homogeneous suspensions. Unlike many studies, no surfactant is used for the fuel blending, because this project intends to directly compare the difference of engine performance between nano additive modified fuels and neat fuels, where the existence of surfactant would influence the result of the comparison. After standing for one day, the blended fuels are moved to the fuel tank of the constant volume vessel (CVV) system. The suspensions can stay stable and no deposition occurs after one week, and 40 ppm is the maximum value we find which can maintain the blends stable for such long time. Pure DF and GTL are used as references. These nano additives modified fuels (nano-fuels) are named as DF-Ce25, DF-CNT, GTL-Ce25 and GTL-CNT respectively. The main physical properties are summarised in Table 2.

2.2. Spray experiment system

As shown in Fig. 1, the spray experiment system consists of a fuel feed system, an optical diagnostic device, a cooling system and a constant volume vessel (CVV). The fuel is delivered by a pump and then a common rail, which enables a maximum fuel pressure of 1800 bar. It then reaches a 0.16 mm single-hole injector to generate fuel spray in the CVV.

The CVV has a volume of 5.65 L. A 4.5 kW ceramic band heater is adhered to the external surface of the vessel wall to increase the internal ambient temperature. Four fused silica 90 mm windows are fitted for optical diagnostics. A three-blade impellor is installed at the bottom for internal agitation and is externally driven by a Micro Mag Drive motor.

Table 2
Physical properties of nano additive modified fuels.

Fuel	Density at 15 °C (kg/m^3)	Viscosity at 40 °C (mPa·s)	Surface tension at 20 °C (mN/m)	LHV (kJ/kg)	Thermal conductivity (W/kg/K)	Specific heat at 40 °C (J/kg/K)	CN	Distillation values
DF	840.4	2.82	28.9	42,853	0.126	2358	54.2	See Table A1 in Appendix
DF-Ce25	840.4	2.81	28.9	42,853		1926		
DF-CNT	840.4	2.77	28.9	42,853		2037		
GTL	780	2.72	28.0	43,600	0.134	2260	73	See Table A1 in Appendix
GTL-Ce25	780	2.71	28.0	43,600		2015		
GTL-CNT	780	2.65	28.0	43,600		1843		

The density, LHV, surface tension and 100% distillation temperature are provided by Coryton. The specific heat and the viscosity are measured by NDJ-9S and NETZSCH DSC 214, respectively. The cetane number and thermal conductivity of DF and GTL are from [27,28].

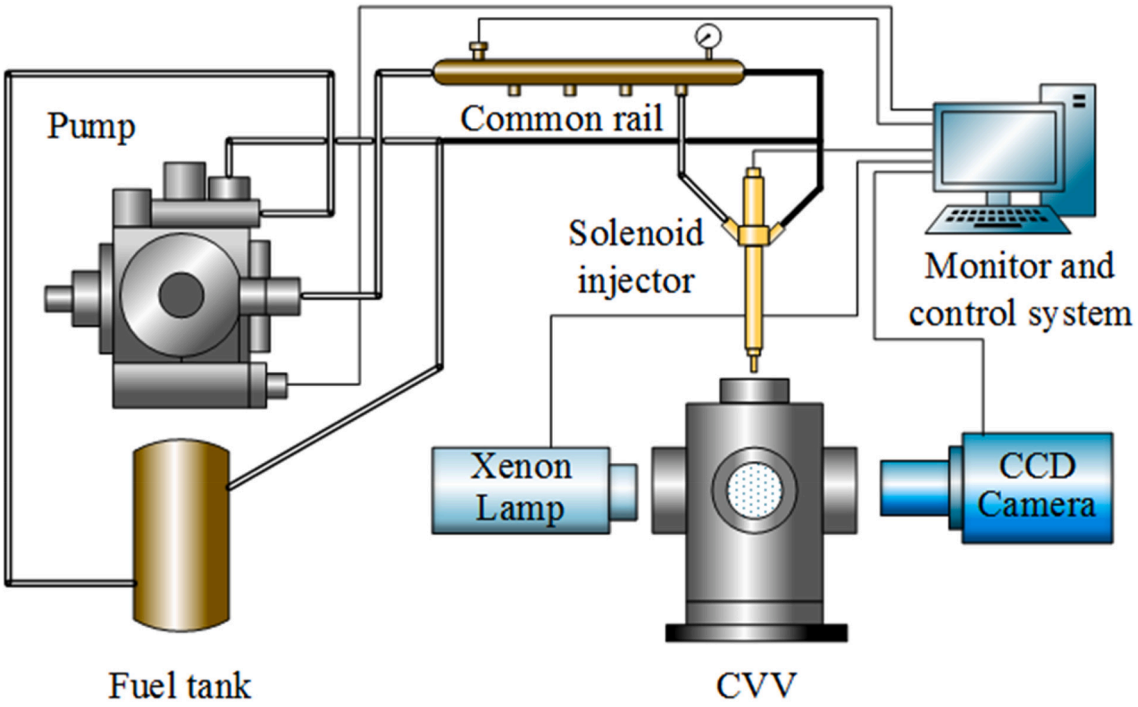

Fig. 1. Schematic spray experiment system [29].

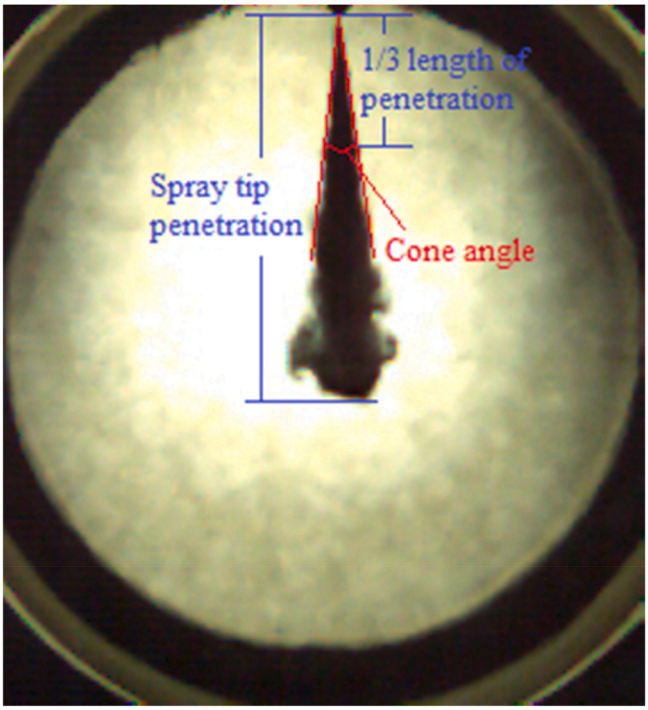

Fig. 2. Illustration of spray penetration and cone angle.

A nitrogen bottle pressurises the internal gas to a maximum of 70 bar, which is measured by a Grems 3100b pressure transducer with an accuracy of 1.5%. 1 mm K-type thermocouples are employed to monitor the internal temperature, the window temperature and the heater temperature with an accuracy of 0.75%.

A PHANTOM V710 CCD camera and a Nikon AF Zoom-Nikkor 24–85 mm f/2.8-4D lens are employed to observe the liquid spray tip penetration and cone angle during experiments with background light provided from a 100 W Xenon lamp. The camera view is set to the resolution of 256 × 272 pixels. The sampling rate and exposure time are 50,000 fps and 19 μs, so the spray image can be recorded every 0.02 ms. During experiments, the injection duration is set to 0.6 ms, which is defined between the start of injection (SOI) and the end of injection (EOI). The SOI is the moment in which the fuel can be viewed, and the EOI is the moment when the spray tail no longer touches the injector tip. We define the periods before and after the EOI as injection and post-injection respectively. The total duration for sampling is 1 ms. Fig. 2 illustrates the definition of spray penetration and the cone angle [30].

The system is cooled by a LAUDA Ultracool UC4 process circulation chiller, which provides water at 15℃ flowing through jackets around the windows, the seal and the motor to absorb heat and then return to the water tank.

2.3. Description of the engine test rig

The engine experiment is conducted on a Cummins ISB4.5 heavy-duty four-stroke diesel engine, as shown in Fig. 3. The specifications of the engine are listed in Table 3.

A DSG 230 kW eddy current dynamometer is implemented to control the engine speed and torque. The crank angle is recorded every 0.5° using an AVL 365C crank angle encoder located at the crankshaft. An AVL pressure transducer QC34C is employed to measure in-cylinder pressure in the third cylinder. A Promass Coriolis flowmeter monitors the fuel mass flow rate. A Horiba MEXA 1600D gas analyser and a Horiba SPCS 1000 particle counter are used to obtain the concentration information of carbon monoxide (CO), nitrogen oxides (NO_x), unburnt hydrocarbons (HC) and particle number (PN) respectively. The whole test rig is cooled by a water cooling system.

2.4. Data processing

The brake specific fuel consumption (BSFC) is the ratio of the fuel mass flow rate to engine brake power. The specific emissions with the unit of g/kWh and #/kWh respectively can be obtained through the following equations.

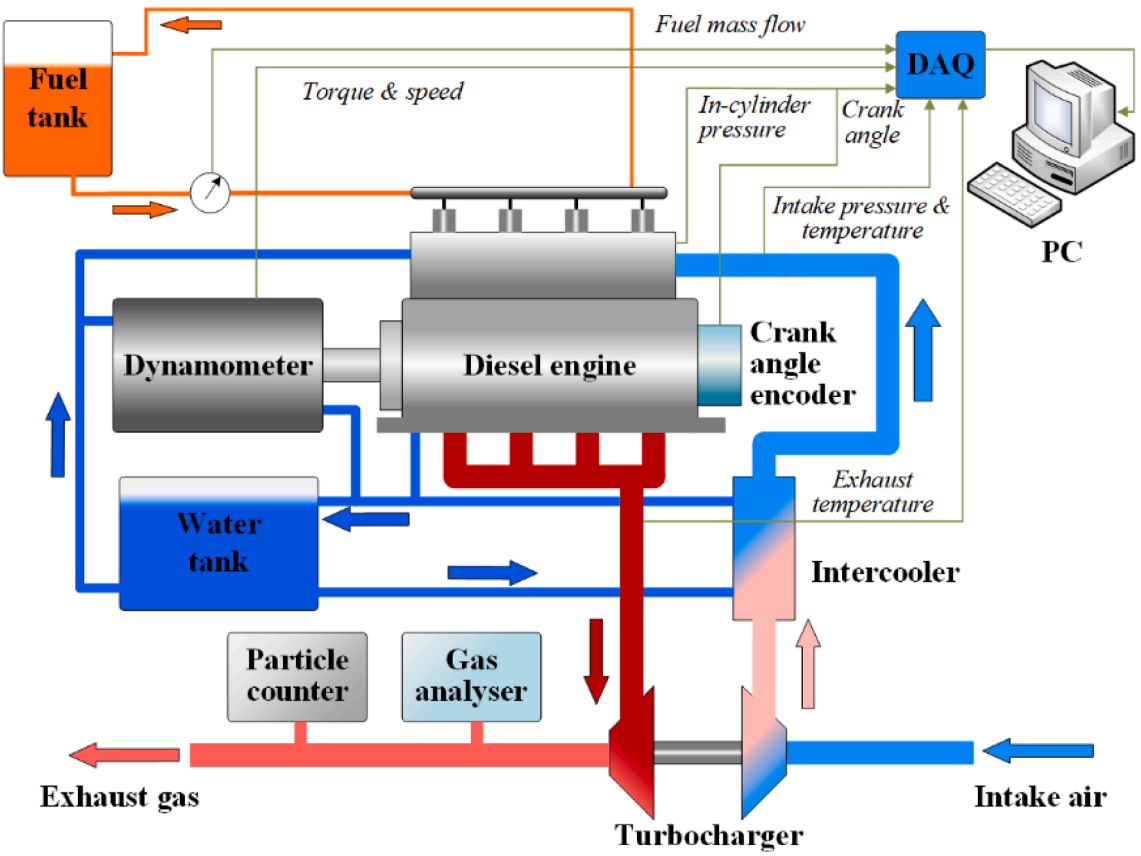

Fig. 3. Schematic diagram of the engine test rig [31].

Table 3
Engine specifications.

Parameter	Value
Model	ISB4.5
Displacement (L)	4.5
Number of cylinders	4
Stroke length (mm)	124
Bore size (mm)	107
Compression ratio	17.3
Injection method	Common rail direct injection
Injection pressure (bar)	1800 bar
Injector type	Solenoid eight-hole injector
Aspiration	Wastegate turbocharger
Speed (rpm)	800 ~ 2500
Torque (Nm)	Max 760 at 1400 ~ 1800 rpm
Power (kW)	Max 152 at 2300 rpm
Emission standard	Euro V

$$CO_S = \frac{0.000966 \cdot c_{CO} \cdot m_g}{Power} \quad (1)$$

$$NO_{xS} = \frac{0.001587 \cdot c_{NO_x} \cdot m_g}{Power} \quad (2)$$

$$HC_S = \frac{0.000479 \cdot c_{HC} \cdot m_g}{Power} \quad (3)$$

$$PN_S = \frac{c_{PN} \cdot m_g \cdot 10^6}{Power \cdot \rho_g} \quad (4)$$

Here c refers to the concentration (ppm and #/cm^3), *Power* is the engine brake power, m_g stands for the exhaust flow rate (kg/h), and exhaust density $\rho_g = 1.293$ kg/m^3.

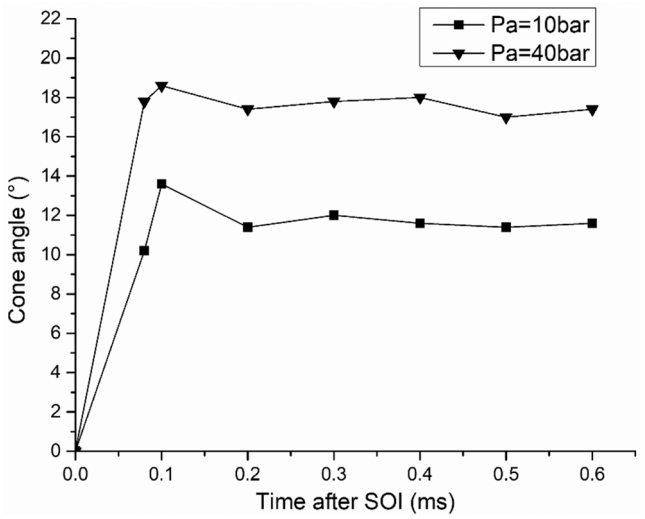

Fig. 4. Cone angle of DF at 1800 bar rail pressure, 600 K ambient temperature and various ambient pressure.

2.5. Experimental conditions

Firstly, spray experiments of DF, DF-Ce25, DF-CNT, GTL, GTL-Ce25 and GTL-CNT are conducted to compare their spray characteristics at 1800 bar rail pressure, 600 K ambient temperature with the ambient pressure varying from 10 bar to 40 bar.

Then, spray experiments on pure DF are conducted to analyse the influence of rail pressure (P_r), ambient pressure (P_a) and ambient temperature (T_a) at 64 different conditions. The rail pressure, amibient

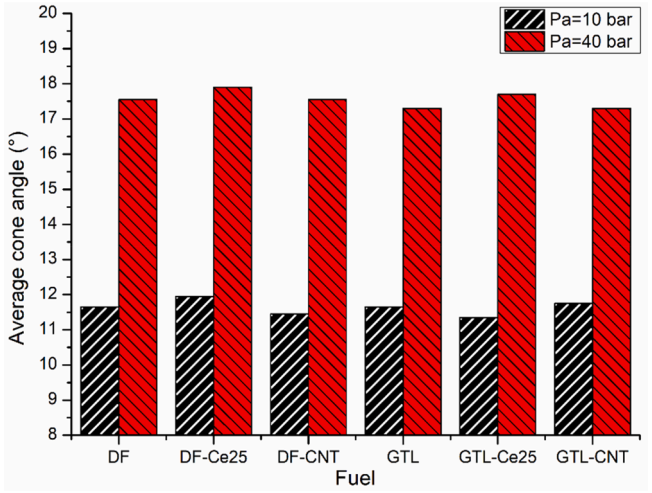

Fig. 5. The average cone angle of nano additive modified fuels.

pressure and ambient temperature are selected in the ranges of 900 K ~ 1800 K, 10 bar ~ 40 bar and 303 K ~ 600 K, respectively. Their values and combinations in all the conditions are listed in Table A2 in Appendix, which are confirmed by the Design of Experiments (DoE).

In terms of engine experimental conditions, the engine is running at 1500 rpm speed and 200 Nm torque for 120 s for each fuel. Experiments on each fuel are repeated three times to obtain the error bar.

3. Results and discussions

3.1. Comparisons among nano-fuels

Spray penetration and cone angle are two representative macroscopic spray characteristics, which are related to droplet breakup and evaporation. In the breakup process, droplets are subjected to two groups of forces. One is the dynamic drag force generated by the momentum of droplets and the density of the internal gas. The other is the viscosity and surface tension of the droplets. Droplets start to break up when the two groups of forces become imbalanced. A larger cone angle usually indicates a stronger breakup, whilst higher velocity of droplets and higher fuel properties such as density, viscosity and surface tension lead to greater spray penetration.

Fig. 4 is an a graph showing cone angle against time at 1800 bar rail pressure and various ambient conditions, where the cone angle at all conditions experiences a dramatic jump to the peak at about 0.1 ms after the SOI, and then fluctuates slightly but stays relatively stable until the EOI. According to Ref [32], the peak cone angle occurs as a result of the breakup time, when the spray forms a blob-like shape. After breakup time, the spray becomes relatively stable for a period during the injection (about 0.2 ~ 0.6 ms). Accordingly, we introduce the average cone angle as a measure of spray quality in this experiment, which is the mean value of the cone angle between 0.2 ms and 0.6 ms.

In order to investigate the effect of both breakup and evaporation on spray for different fuels, the experiments are conducted at 1800 bar rail pressure, 600 K ambient temperature, and the ambient pressure of 10 bar and 40 bar respectively. Therefore, the average cone angle and spray penetration are obtained for both neat fuels and nano additive modified fuels.

As illustrated in Fig. 5, the average cone angle of all test fuels are very close and the variance is within 1° at each ambient pressure. As mentioned above, the cone angle is largely determined by the break-up but also marginally influenced by droplets evaporation. The result indicates that the addition of CeO_2 nanopowder and CNT has no comparable impact on breakup and evaporation for either DF or GTL during the injection period, and thus cannot significantly change the average cone angle.

As shown in Fig. 6, DF and its nano additive modified fuels always have larger spray penetration than GTL the associated modified fuels. The reasons are twofold: First, DF has the higher density and viscosity, which enable larger droplets and to penetrate longer. Second, GTL has higher thermal conductivity which promote droplets to absorb heat and evaporate faster. In terms of the nano additive modified fuels, they have the same tendency as DF and GTL at 10 bar ambient pressure in spray penetration, which increases with time during the injection and then drops to zero in post-injection. Moreover, during the injection period, the penetration of nano additive modified DF is smaller than that of DF due to the differences in their thermal conductivity, specific heat and viscosity. As mentioned in Table 1 and Table 2, nano additives have significantly higher thermal conductivity than fuels, and thus the nano additive modified DF has higher thermal conductivity than DF. Consequently, the lower viscosity of nano additive modified DF result in smaller droplets, and the higher thermal conductivity as well as lower specific heat enable higher temperature rise and faster evaporation when absorbing heat, which contributes to smaller penetration. In contrast, the difference between GTL and nano additive modified GTL is tiny during injection, because GTL has lower viscosity and higher thermal conductivity than DF. As a result, the difference in these properties between the nano additive modified GTL and net GTL is smaller than that between the nano additive modified DF and net DF, which induces close penetrations for GTL and its nano additive blend.

In the post-injection period, the penetration of DF-CNT and GTL-CNT

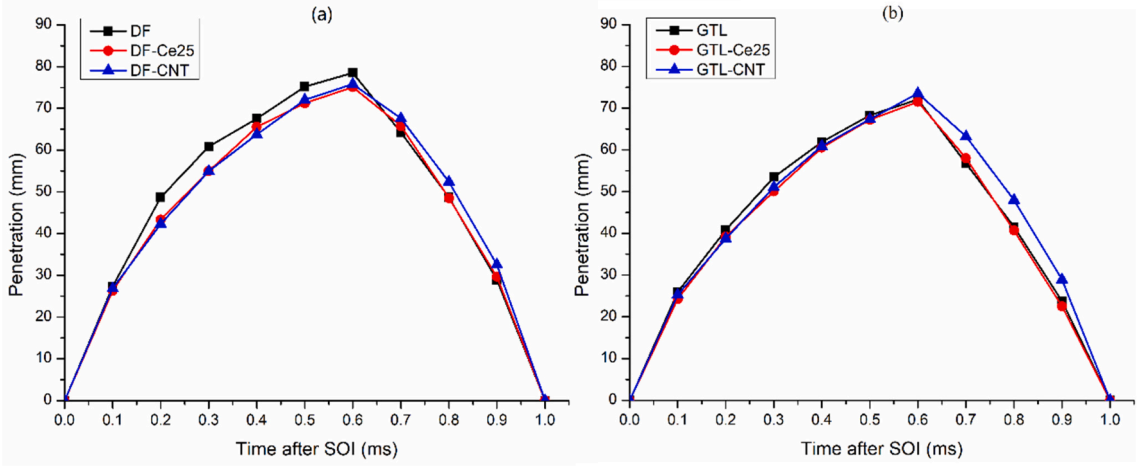

Fig. 6. Spray penetration of nano additive modified fuels at 10 bar ambient pressure.

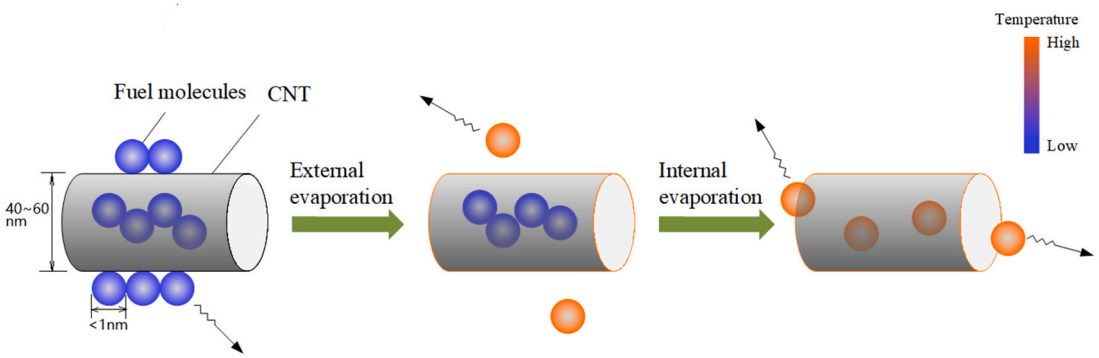

Fig. 7. Evaporation of GTL-CNT [31].

becomes slightly greater than that of other fuels due to the structure of CNT. Although blending CNT increases the thermal conductivity of net fuels, some fuel molecules stay inside the CNT because it is a long pipe with thick wall. Consequently, the fuel inside can only evaporate via the two ends of CNT instead of in all directions, which slows down the entire evaporation process, as shown in Fig. 7. Conversely, due to the small amount of additive of CNT, the amount of fuel molecules inside the CNT is low. Therefore, the evaporation rate of all the fuels containing CNT is only slightly reduced. Given lower thermal conductivity and higher specific heat of DF than GTL, the reduction in evaporation rate between DF and DF-CNT is even less significant compared with that between GTL and GTL-CNT.

When the ambient pressure rises to 40 bar, the difference between neat fuels and modified fuels is negligible during the injection as shown in Fig. 8, because the higher ambient pressure enhances the breakup of droplets which makes the impact of fuel properties insignificant. In the post-injection period, the penetration of DF and its modified fuels keeps gradually increasing with no difference between the fuels, whilst that of GTL and its modified fuels starts to drop and GTL-CNT has overall larger penetration than others. This phenomenon can most likely be attributed to the higher thermal conductivity and lighter compositions of GTL which improve the influence of evaporation.

3.2. *Influence of experimental conditions of the spray of DF*

In order to study the influence of experimental conditions on spray characteristics, DF is employed as the test fuel, as its physical properties are well known.

Fig. 9 indicates two features for the average cone angle. First, the average cone angle at the same ambient conditions is very similar regardless of varying rail pressure. It agrees with the conclusion in the literature [33], where the cone angle is demonstrated stable despite varying injection pressures. Second, the value of the average cone angle grows significantly at increased ambient pressure, and the level of increase seems not to remain at most ambient temperatures and rail pressures. This is because ambient pressure dominates the breakup of liquid fuel, and thus higher ambient pressure promotes a fuel to break up into smaller droplets, due to stronger impinging and friction between the fuel and ambient gas (nitrogen).

In terms of ambient temperature, the average cone angle reduces slightly when the ambient temperature increases, which is mainly caused by the enhanced evaporation around the boundary of the spray at high-temperature conditions. However, the extent of reduction in average cone angle is related to the rail and ambient pressures. When ambient pressure is 10 bar, the average cone angle experiences more reduction at higher rail pressures. At 40 bar ambient pressure, the reduction in average cone angle is also promoted by increasing rail pressure, but its dropping rate is slower compared with the situation of 10 bar ambient pressure. This means the influence of rail pressure on the evaporation of droplets is more significant at reduced ambient pressure due to the larger surface of spray boundary, which enables more fuel droplets to absorb heat from hot ambient gas.

Figs. 10–12 show the spray penetration against sample time under all ambient conditions (P_a and T_a) at the rail pressure (P_r) of 900 bar, 1200

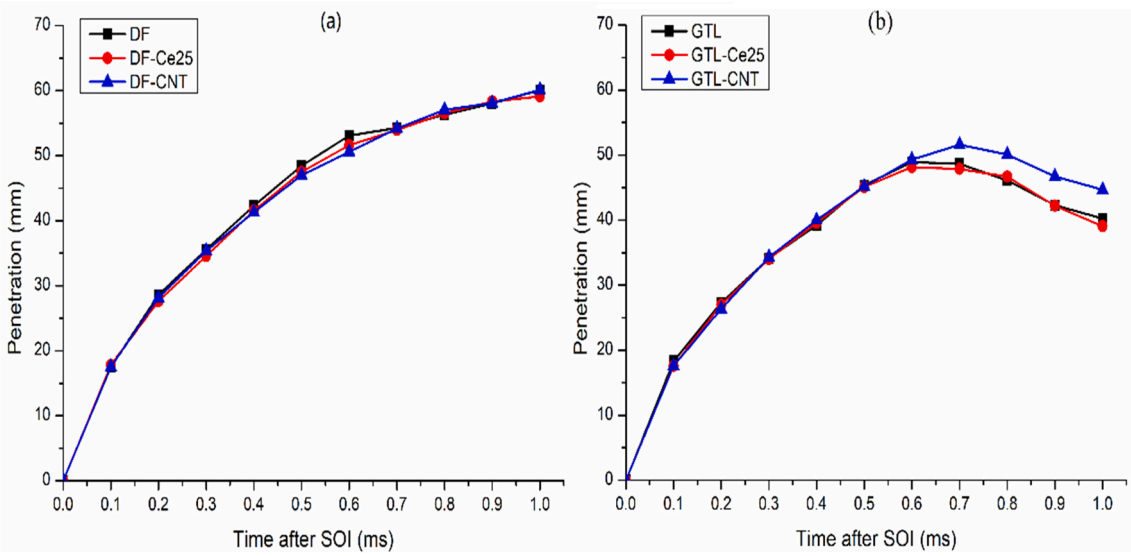

Fig. 8. Spray penetration of nano additive modified fuels at 40 bar ambient pressure.

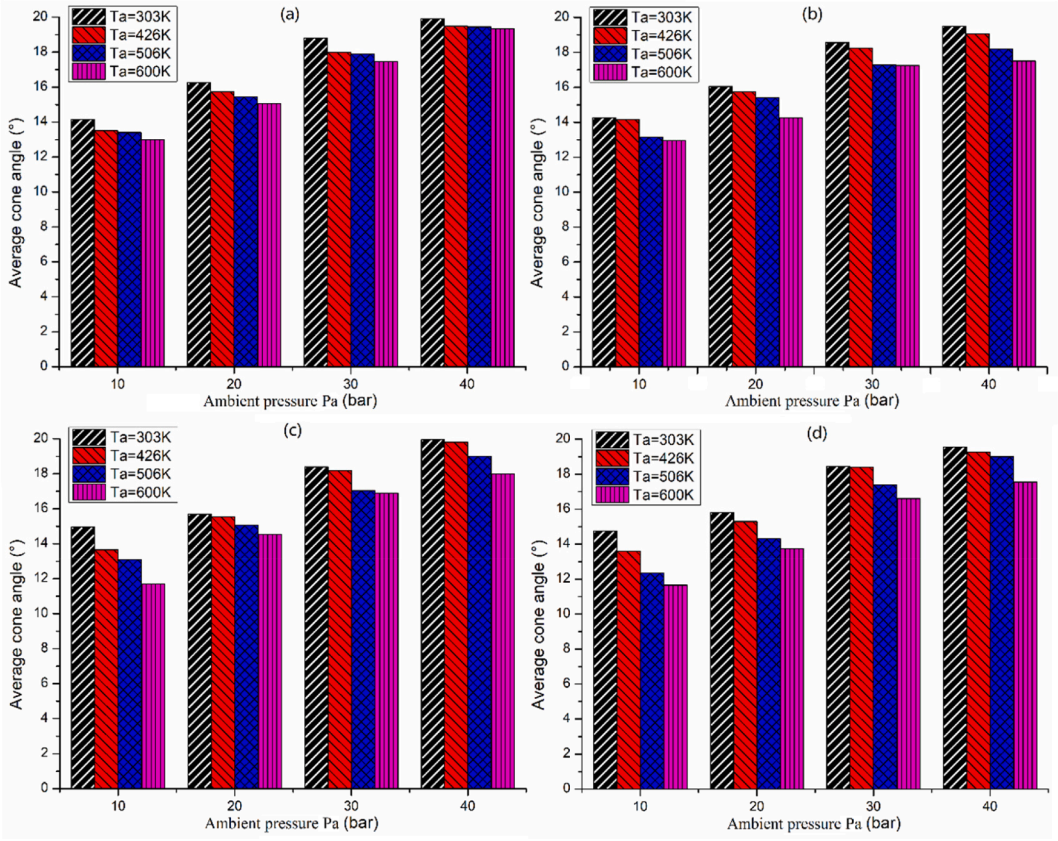

Fig. 9. The average cone angle of diesel fuel at various ambient conditions and rail pressure of 900 bar (a), 1200 bar (b), 1500 bar (c) and 1800 bar (d).

bar, 1500 bar and 1800 bar, respectively. Only the results at two representative ambient temperatures 303 K and 600 K are shown here. The results at all ambient temperatures are given in Appendix.

As shown in Figs. 10–13, the spray penetration in the injection and post-injection periods has different tendencies. During the injection, the spray penetration is increasing with sampling time under all ambient pressures at cold conditions. However, the penetration of low ambient pressure (10 ~ 20 bar) tends to drop around the end of injection (about 0.5 ~ 0.6 ms) when the ambient temperature is high (506 ~ 600 K), especially at low rail pressure. The reasons are twofold: first, the sharp and long penetration at low ambient pressure has a larger surface of spray boundary, and thus absorbs heat faster to evaporate in the hot ambient gas; second, lower ambient pressure means the ambient gas has lower density and hence aides evaporation. According to Ref [34], the impinging effect is predominant during the breakup. Therefore, the spray penetration is always much smaller at higher ambient pressure than that at lower ambient pressure at all ambient temperatures, because the stronger interaction between ambient gas and fuel significantly enhances the breakup of droplets.

In post-injection, the impact of ambient temperatures becomes more significant. At 300 K, penetrations at all ambient pressures keep increasing regardless of different rail pressures, and the penetrations at lower ambient pressure are all shorter than that at the higher pressure. As the evaporation effect is insignificant at low-temperature conditions and the fuel droplets can only move downstream, driven by inertia, the ambient pressure still dominates the post-injection period. When the

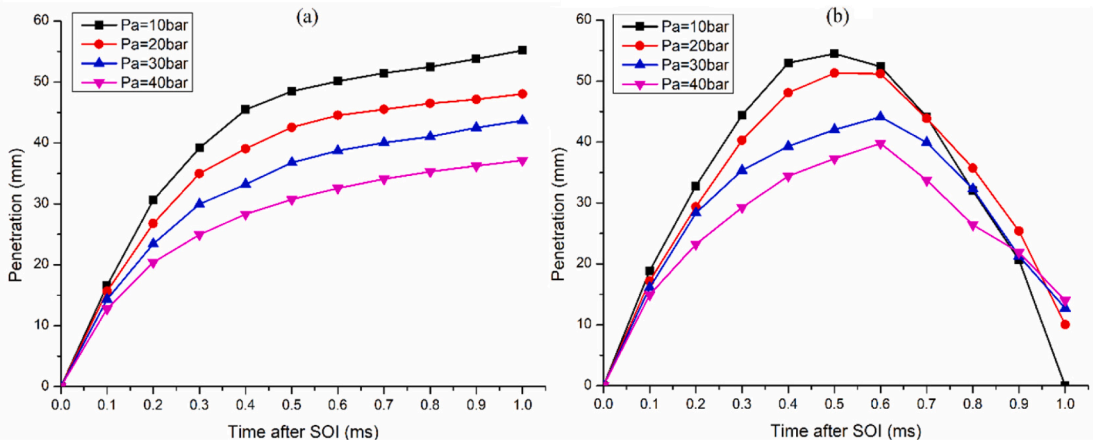

Fig. 10. Effect of P_a on spray penetration of DF at 900 bar P_r and the T_a of 303 K (a) and 600 K (d).

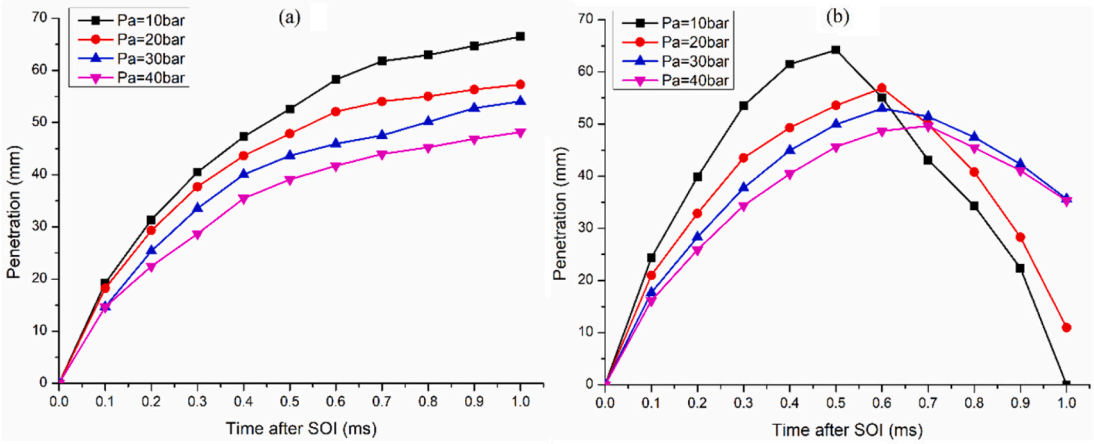

Fig. 11. Effect of P_a on spray penetration of DF at 1200 bar P_r and the T_a of 303 K (a) and 600 K (d).

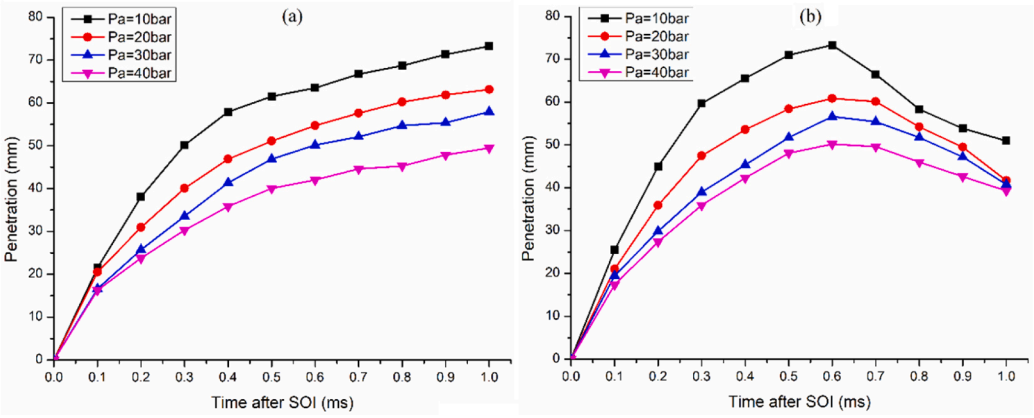

Fig. 12. Effect of P_a on spray penetration of DF at 1500 bar P_r and the T_a of 303 K (a)and 600 K (d).

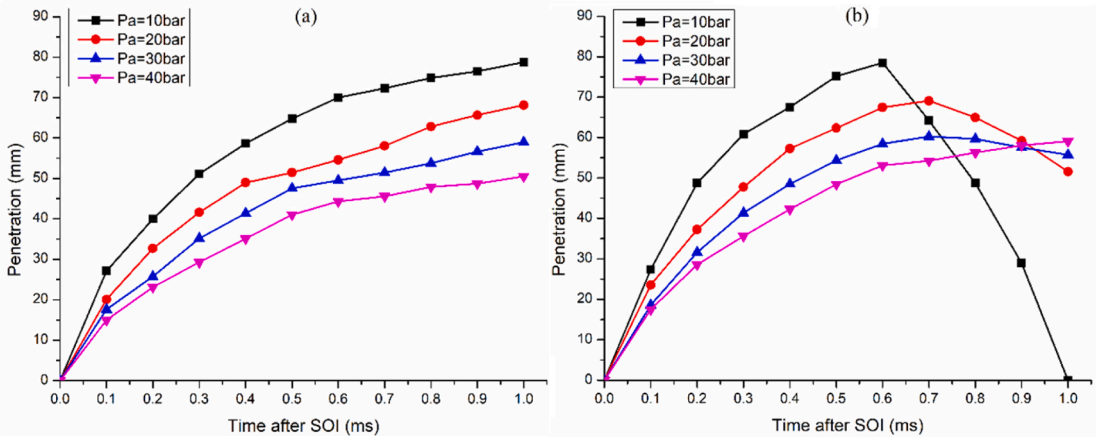

Fig. 13. Effect of P_a on spray penetration of DF at 1800 bar P_r and the T_a of 303 K (a)and 600 K (d).

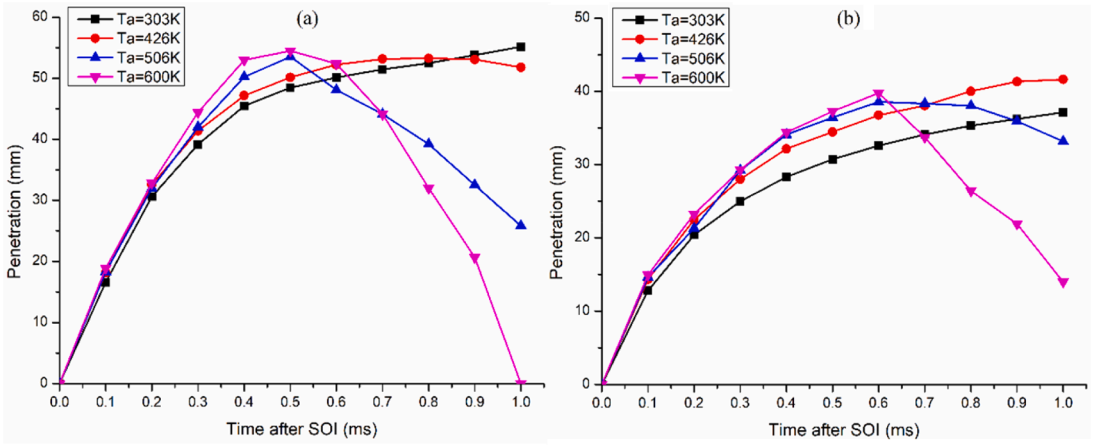

Fig. 14. Effect of T_a on spray penetration of DF at 900 bar P_r and P_a of 10 bar (a) and 40 bar (d).

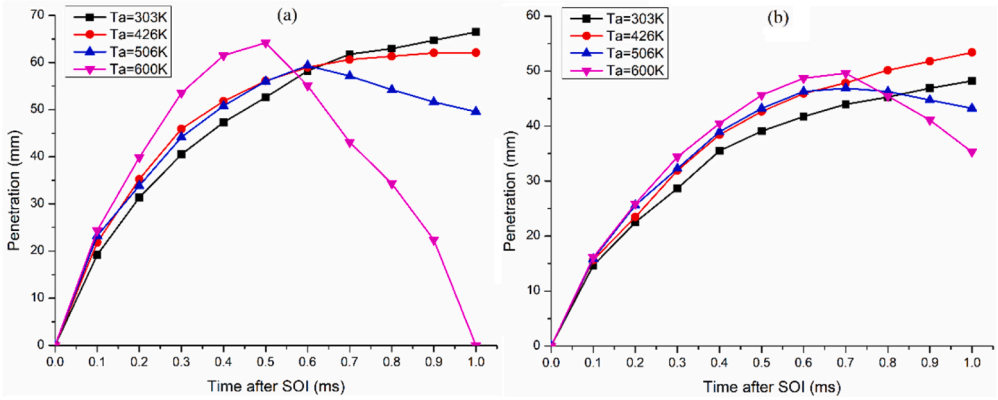

Fig. 15. Effect of T_a on spray penetration of DF at 1200 bar P_r and P_a of 10 bar (a) and 40 bar (d).

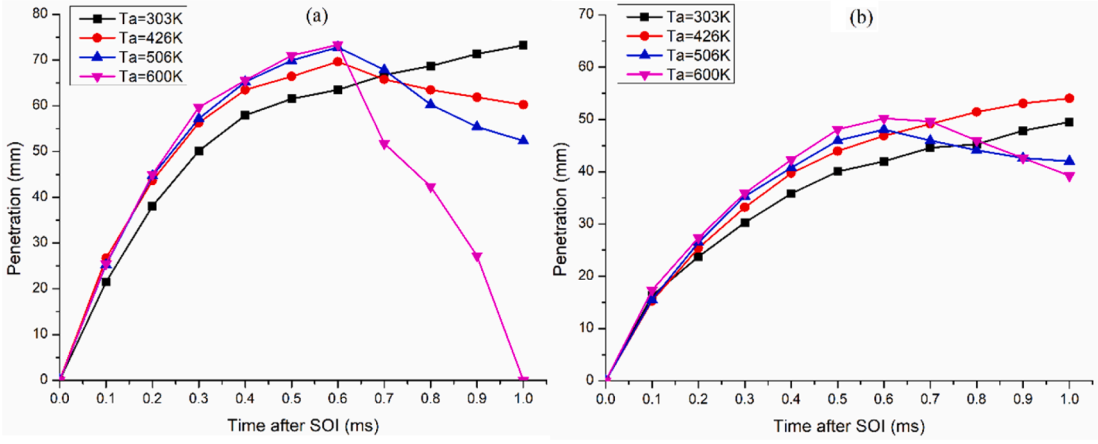

Fig. 16. Effect of T_a on spray penetration of DF at 1500 bar P_r and P_a of 10 bar (a), 20 bar (b), 30 bar (c) and 40 bar (d).

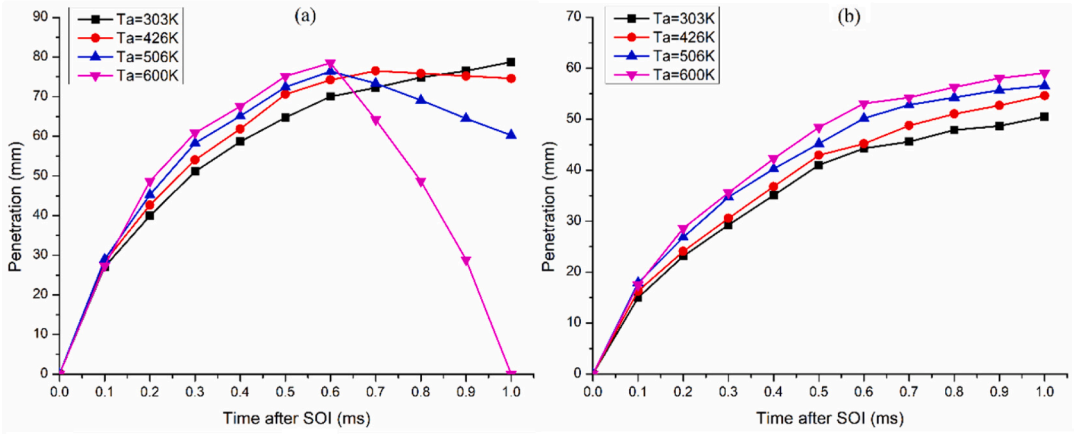

Fig. 17. Effect of T_a on spray penetration of DF at 1800 bar P_r and P_a of 10 bar (a)and 40 bar (d).

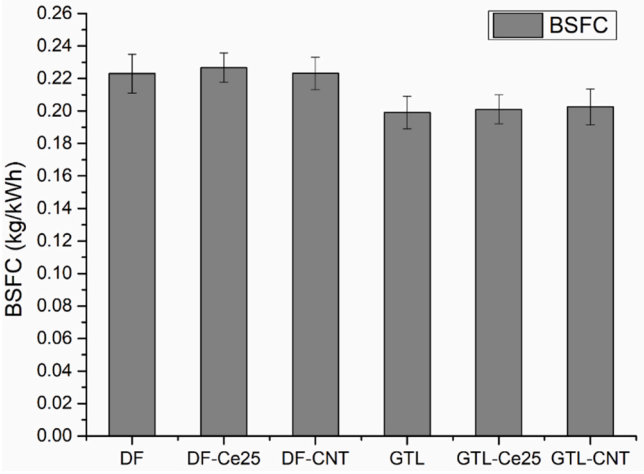

Fig. 18. BSFC of nano additive modified DF and GTL.

ambient temperature rises, penetrations at all ambient pressures and rail pressures start to reduce with time, and the penetration reductions occur earlier when there are lower ambient and rail pressures. Consequently, penetrations at 10 and 20 bar ambient pressure sometimes even drop shorter than those at 30 and 40 bar, such as those shown in Fig. 10 (c) and Fig. 10 (d). This phenomena indicates that evaporation is predominant during post-injection in hot conditions whilst the ambient pressure becomes insignificant because the velocity of droplets is low in this period, due to the absence of rail pressure.

In order to further study the impact of ambient temperature, Figs. 14-17 are shown to illustrate the spray penetration at varying ambient temperature (T_a) during the sample time. Only two representive ambient pressures (P_a) are shown here. The results at all ambient pressures are given in Appendix.

In the injection, penetrations at the most ambient pressures increase at higher ambient temperature regardless of different rail pressure. This indicates that the fuel can penetrate further when the ambient temperature is higher because the ambient gas density drops at increased temperature and fixed pressure. As a result, the drag force on droplets is weakened and leads to a larger penetration. However, the penetration under 900 bar rail pressure starts to drop with sample time at a high ambient temperature around the end of injection (0.5 ~ 0.6 ms), because the small amount of injected fuel and lower velocity of droplets enables faster evaporation. Therefore, penetrations under a rail pressure higher than 900 bar can still maintain growth until the EOI.

In post-injection, the penetration keeps growing at 40 bar ambient pressure and 1800 bar rail pressure. In contrast, the penetration starts to drop with increasing ambient temperature at ambient pressure of 30 bar and less, and the reduction rate of penetration at increased ambient temperature becomes greater compared to that at reduced temperatures. Furthermore, when the rail pressure drops to lower than 1800 bar, the penetration is reduced by increased ambient temperature, regardless of ambient pressure. This indicates that the ambient temperature is

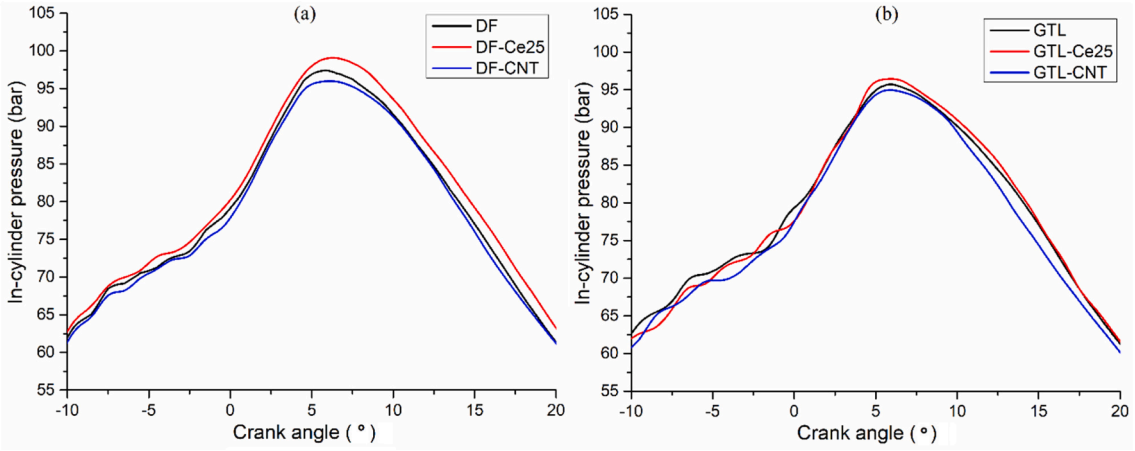

Fig. 19. In-cylinder pressure of nano additive modified DF (a) and GTL (b).

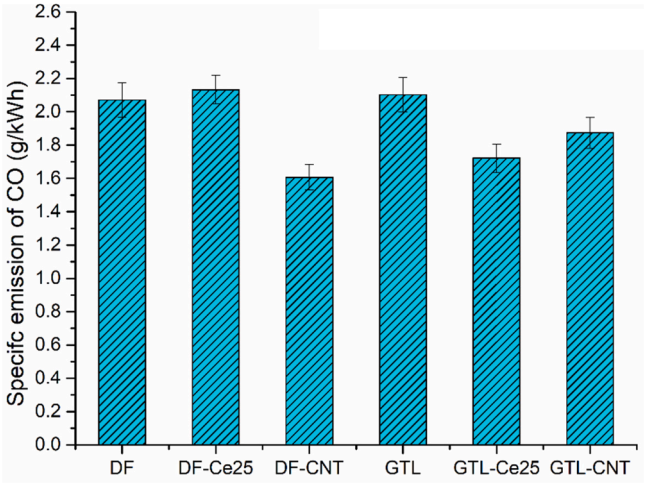

Fig. 20. Specific emission of CO of nano-fuels.

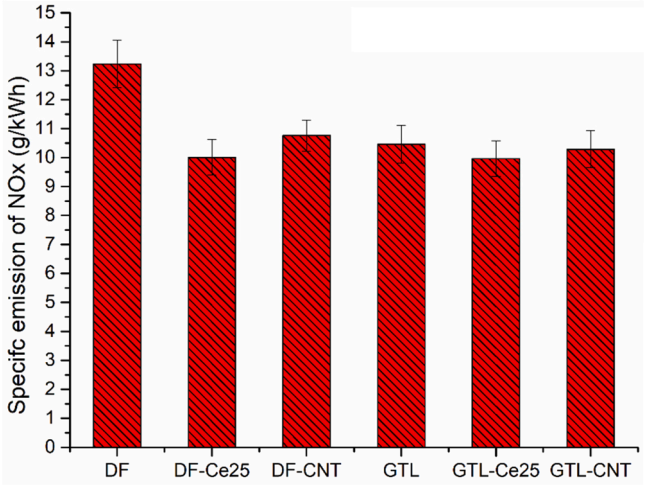

Fig. 21. Specific emission of NO_x of nano-fuels.

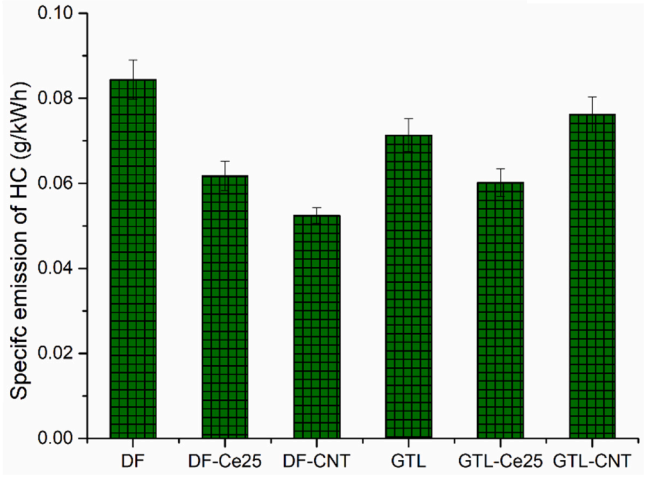

Fig. 22. Specific emission of HC of nano-fuels.

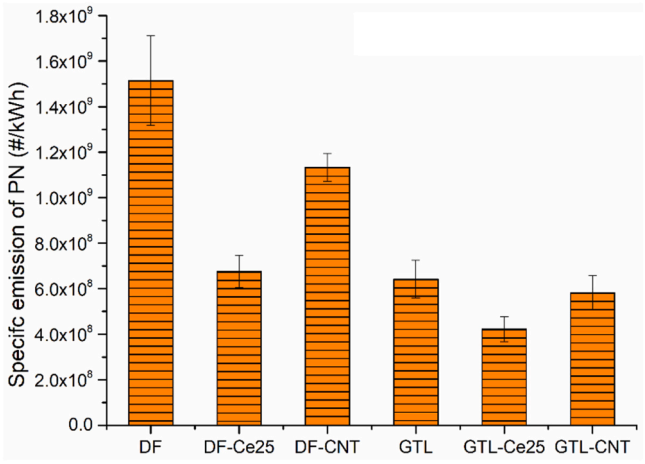

Fig. 23. Specific emission of PN of nano-fuels.

predominant after the injection and its influence can be enhanced by reducing rail and ambient pressures because droplets have a lower velocity at these conditions and thus are not capable of breaking up in a post-injection period. Therefore, they only evaporate into the ambient gas. Moreover, the spray at low ambient pressures is sharper and longer and thus has a larger surface of boundary to evaporate, which makes the penetration drop faster.

3.3. Engine performance of nano additive modified fuels

The engine performance including the BSFC, in-cylinder pressure curve, and pollutant emissions are obtained at 1500 rpm speed and 200 Nm torque. Fig. 18 illustrates the BSFC of all test fuels at the engine condition. GTL and the nano additive modified GTL fuels all have reduced BFSC (by about 10%) compared to DF and modified DF, caused by higher LHV of GTL. In contrast, nano additives alone seem to have no impact on BSFC.

As shown in Fig. 19, CeO_2 nanopowder modified DF and GTL have higher peaks in in-cylinder pressure than pure GTL and DF. The reasons are twofold. First, CeO_2 nanopowder reduces viscosity and improves diffusivity for these fuels and thus promotes spray, as demonstrated in the spray experiment. Second, CeO_2 nanopowder is an effective catalyst that accelerates the combustion reactions via Equation (5), where CeO_2 converts to Ce_2O_3 through reverse reactions.

$$4CeO_2 \rightleftharpoons 2Ce_2O_3 + O_2 \quad (5)$$

In contrast, reduced in-cylinder pressure is produced by CNT modified fuels compared to neat fuels in the main combustion process, which is probably because the hollow structure of CNT slows down heat absorption and evaporation, as described in the spray experiment. The liquid fuel on the outside wall of CNT is firstly heated by the environment and evaporates. Then the wall of CNT is heated to a higher temperature. Eventually, the fuel inside CNT evaporates after being heated by the hot CNT wall. Due to the thick multi-wall, the fuel inside is heated slower than that outside, and more heat is absorbed by the fuel-CNT mixture. Consequently, the evaporation duration is enlarged, which leads to a lower in-cylinder pressure at the peak.

Fig. 20 shows CO emissions of GTL and DF as well as their blends with nano additives. Although GTL has the higher H/C ratio, it emits nearly the same CO compared to DF. This is mainly because the engine injection strategy is optimised for diesel fuel only and thus GTL is not burnt under its optimal condition. Despite similar levels of CO

emissions, the CO emissions of GTL are significantly reduced by CeO_2 nanopowder, which could be attributed to the oxidization of CeO_2. In contrast, the CO emissions of DF are increased slightly, when DF is blended with CeO_2. Previously, the authors have reported and demonstrated that CeO_2 nanopowder can only reduce CO emissions within a certain range of engine load and speed, which may vary for different fuels [31]. In terms of CNT, CO emissions are reduced for both DF and GTL and this is mainly caused by the improved spray despite its reduced combustion temperature.

As shown in Fig. 21, CeO_2 nanopowder can reduce NO_x emissions for both DF and GTL, because CeO_2 can convert to Ce_2O_3 (Ce^{+3}) and convert back to CeO_2 (Ce^{+4}) at high-temperature conditions. During combustion, CeO_2 promotes the oxidation of unburnt fuel molecules, whilst the Ce_2O_3 can deoxidize some combustion products. For example, NO_x emissions can be consumed through the equation below:

$$Ce_2O_3 + 2NO \rightarrow 2CeO_2 + 1/2N_2 \quad (6)$$

The effect of CNT on NO_x emissions is not as significant as CeO_2 nanopowder, because the reduction of NO_x by CNT is only determined by its lower combustion temperature because of the heat absorption during evaporation. The overall influence of nano additives on GTL is less significant, mainly because the overall emissions level of GTL is already lower than DF.

Compared with the effect of CNT on DF, the effect on GTL is opposite for HC emissions, as GTL-CNT produces more HC than GTL in Fig. 22. CNT has two contradictory effects. Firstly, CNT contributes to lower viscosity and higher thermal diffusivity of fuel, so promotes atomisation and combustion. However, conversely, CNT contributes to lower combustion temperature which is easier for the formation of HC. In this case, it is believed that the reduction of combustion temperature is more significant for GTL in HC formation, as the spray of GTL is already fully developed, compared to DF.

In terms of CeO_2 nanopowder, both GTL-Ce25 and DF-Ce25 experience reduced HC emissions, because CeO_2 acts as the oxidant for HC as shown in Equation (7), and its product Ce_2O_3 deoxidises NO_x.

$$(2x+y)CeO_2 + C_xH_y \rightarrow \left[\frac{2x+y}{2}\right] Ce_2O_3 + \frac{x}{2}CO_2 + \frac{y}{2}H_2O \quad (7)$$

In terms of PN emissions, CNT has two contradictory effects similar to that on HC (see Fig. 23). First, CNT lower combustion temperature, and this prohibits the formation of PM as it is more easily formed in the fuel-rich zones occurring at high-temperature conditions. Second, CNT can be the nucleus for PM formation at high-temperature conditions. Accordingly, CNT can significantly reduce PN emissions for DF, mainly due to its effect on reducing the temperature during spray. In contrast, GTL-CNT has the smallest level of reduction because some CNT contributes to PM formation due to the high combustion temperature.

Compared with CNT, the CeO_2 nanopowder modified fuels produce significantly fewer PN emissions, because CeO_2 nanopowder can reduce PN via two pathways. First, CeO_2 oxidizes PM through Equation (8) after they are formed at high-temperature conditions. Second, CeO_2 oxidizes some HCs before they are dehydrogenated and carbonized to form PM.

$$4CeO_2 + C_{PM} \rightarrow 2Ce_2O_3 + CO_2 \quad (8)$$

4. Conclusions

In this paper, both macroscopic spray characteristics and engine performance are investigated on nano additive modified fuels (DF-Ce25, DF-CNT, GTL-Ce25 and GTL-CNT) to evaluate their capability for engine application. Moreover, the effects of rail pressure, ambient pressure and ambient temperature on spray are also analysed by experiments on the DF. The main results are summarised below:

1. GTL shows a smaller spray penetration than DF during both the injection and post-injection periods due to its lower density, higher thermal conductivity and lower viscosity.
2. Nano additives (CeO_2 nanopowder and CNT) have no significant impact on the average cone angle.
3. Both CeO_2 nanopowder and CNT can reduce spray penetration in the injection period at 10 bar ambient pressure when blending with DF, whilst the effect is less significant when blending with GTL. When the ambient pressure rises to 40 bar, nano additives have no significant influence on the spray penetration of GTL and DF during the injection.
4. During post-injection, CNT always increases spray penetration because the the fuel inside the CNT can only evaporate via the two ends of CNT, which slows down the whole evaporation process. Moreover, the increase in the penetration for GTL is larger than that of DF due to the higher thermal conductivity of GTL.
5. Rail pressure can increase the spray penetration significantly but has no effect on the average cone angle, which can only be reduced significantly by decreasing ambient pressure or increasing ambient temperature.
6. During injection, spray penetration can be significantly reduced by increasing ambient pressure but increased by increasing ambient temperature slightly.
7. During post-injection, ambient temperature is the dominant factor, which enables faster evaporation and thus reduces penetration.
8. CeO_2 nanopowder is a better nano additive, as it can reduce NO_x, HC and PN emissions simultaneously for both DF and GTL. Moreover, its impact on DF is more significant than on GTL.
9. CNT can reduce peak in-cylinder pressure, NO_x and PN for DF, but its effect on GTL is less significant.

CRediT authorship contribution statement

Zhichao Zhang: Conceptualization, Writing – original draft, Writing – review & editing. **Yiji Lu:** Conceptualization, Writing – review & editing, Formal analysis, Supervision. **Zi Qian:** Writing – review & editing, Project administration. **Anthony Paul Roskilly:** Conceptualization, Supervision, Resources.

Declaration of Competing Interest

The authors declare that they have no known competing financial interests or personal relationships that could have appeared to influence the work reported in this paper.

Acknowledgement

This collaborative research project was only possible thanks to generous support from the Royal Academy of Engineering through the Transforming Systems through Partnerships program (TSP1098).

Appendix

(See Figs. A1 – A8, Table A1).

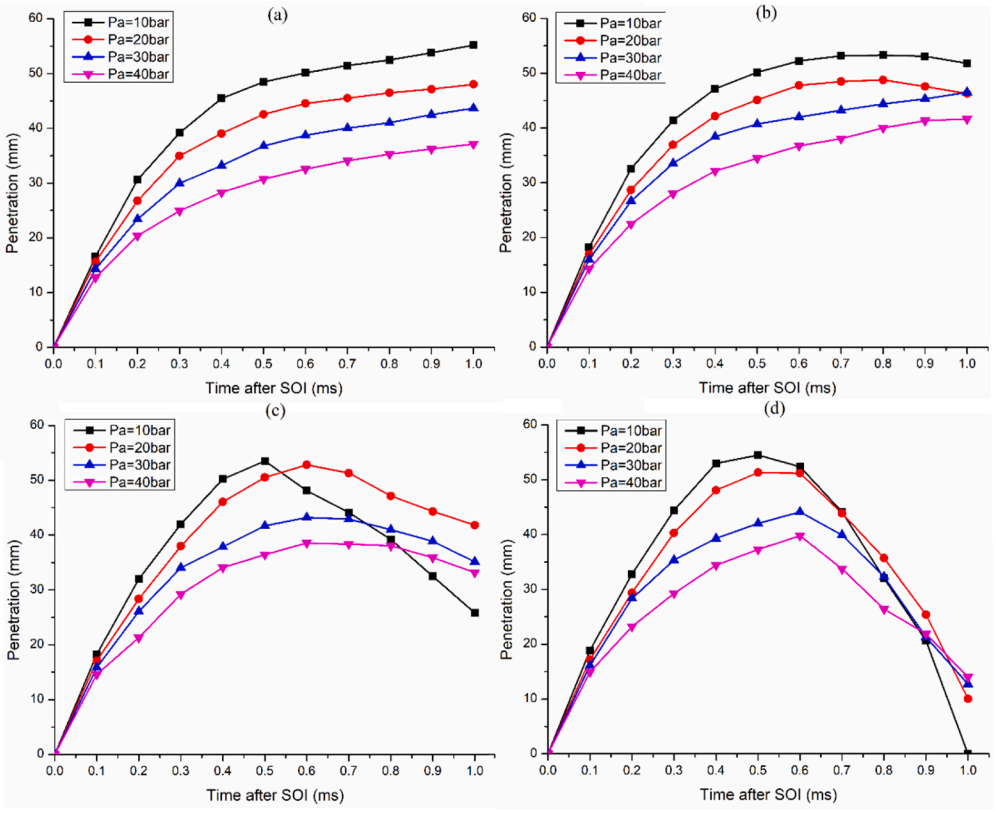

Fig. A1. Effect of P_a on spray penetration of DF at 900 bar P_r and the T_a of 303 K (a), 426 K (b), 506 K (c) and 600 K (d).

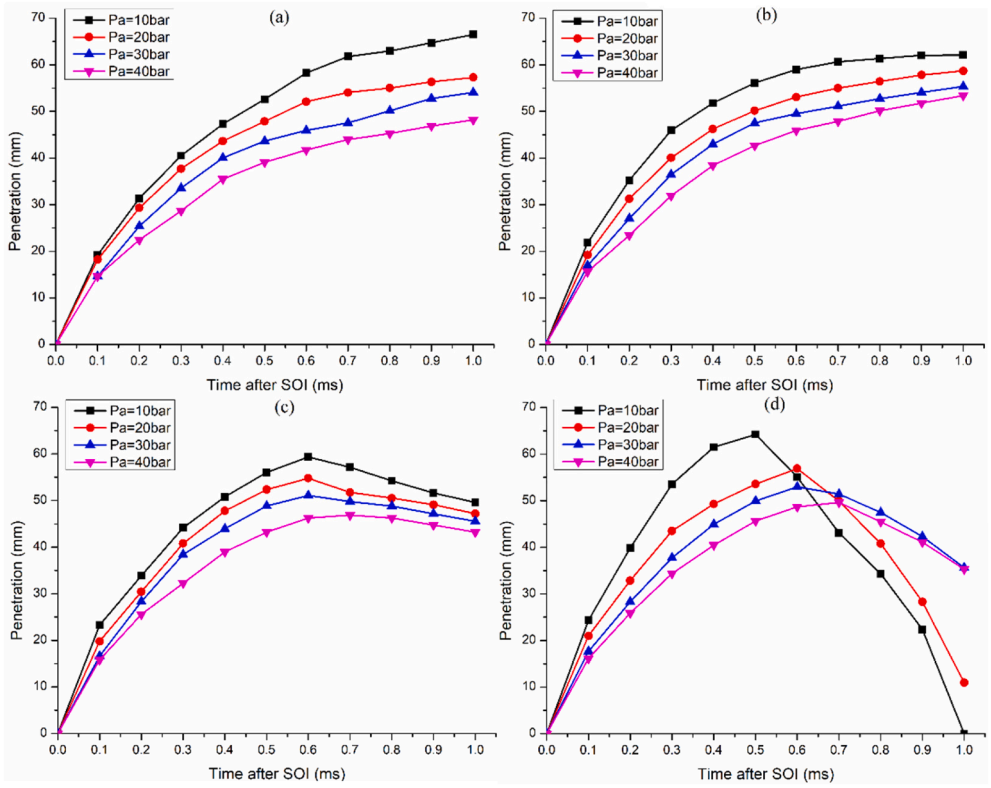

Fig. A2. Effect of P_a on spray penetration of DF at 1200 bar P_r and the T_a of 303 K (a), 426 K (b), 506 K (c) and 600 K (d).

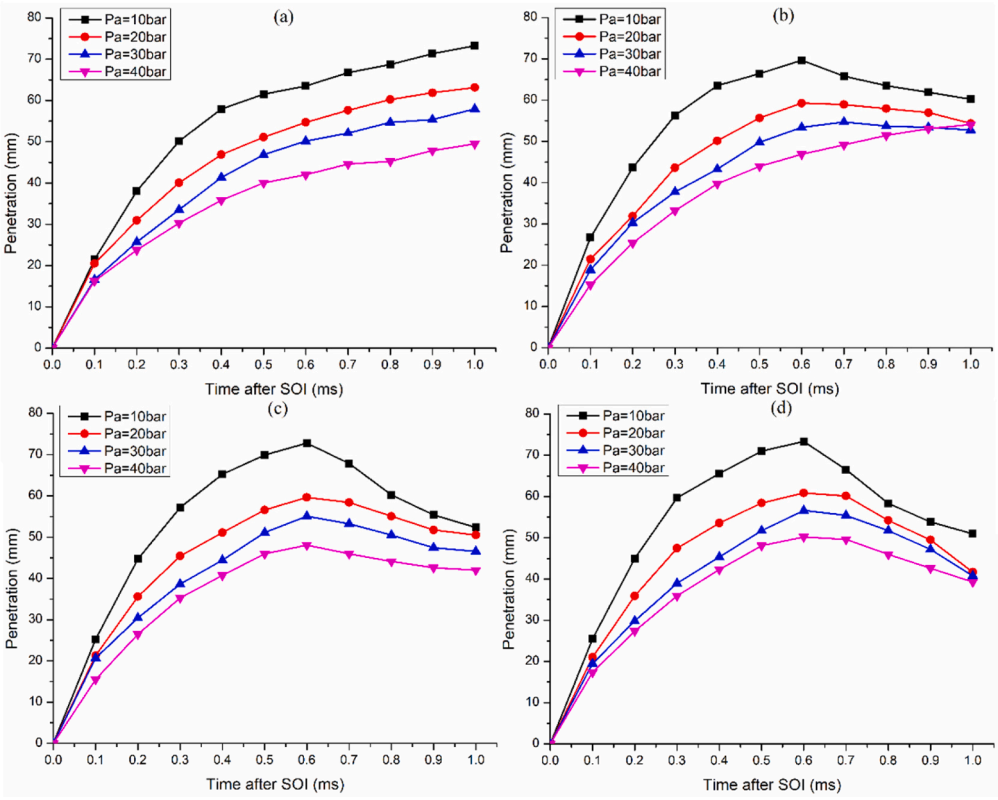

Fig. A3. Effect of P_a on spray penetration of DF at 1500 bar P_r and the T_a of 303 K (a), 426 K (b), 506 K (c) and 600 K (d).

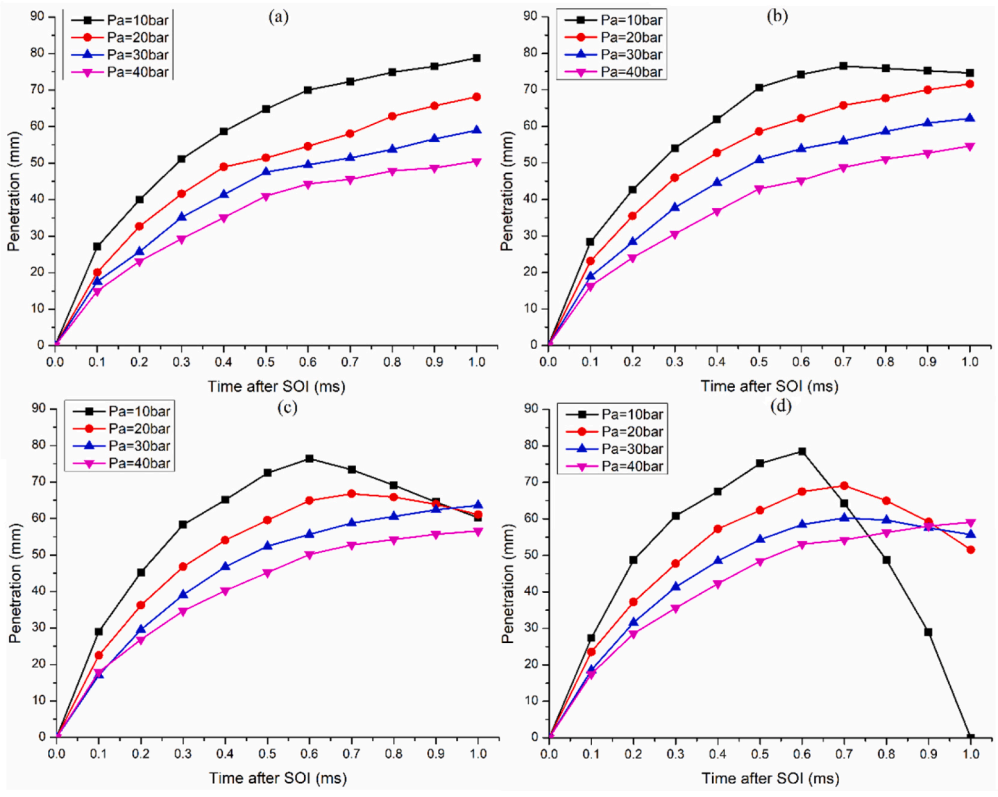

Fig. A4. Effect of P_a on spray penetration of DF at 1800 bar P_r and the T_a of 303 K (a), 426 K (b), 506 K (c) and 600 K (d).

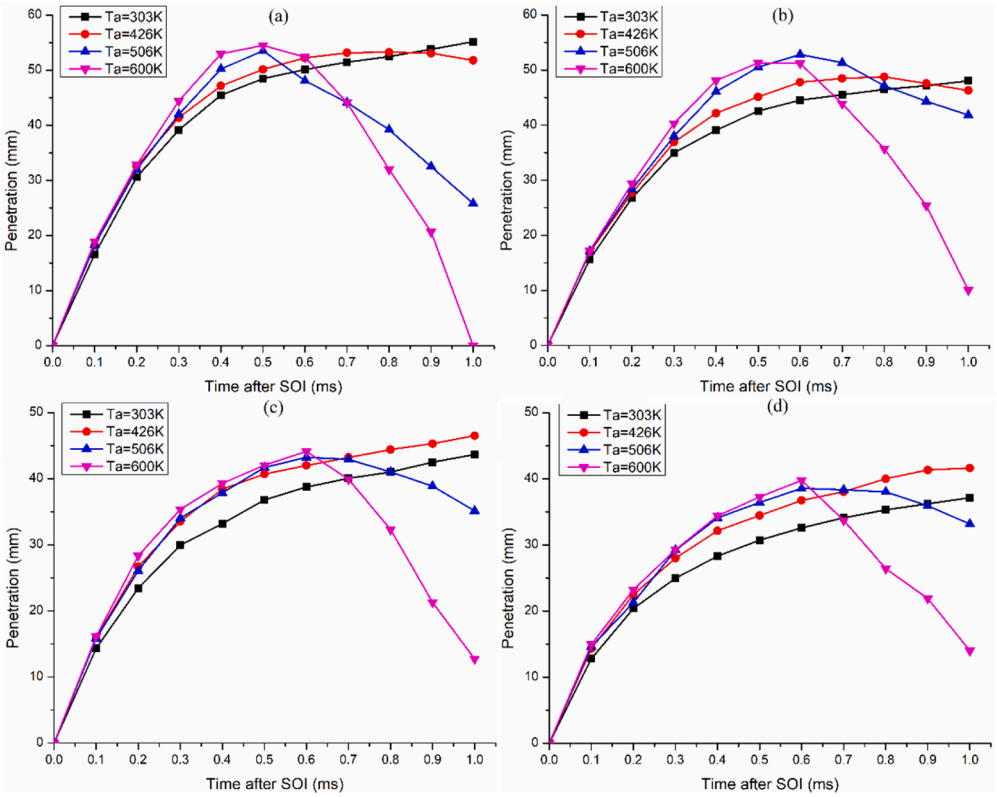

Fig. A5. Effect of T_a on spray penetration of DF at 900 bar P_r and P_a of 10 bar (a), 20 bar (b), 30 bar (c) and 40 bar (d).

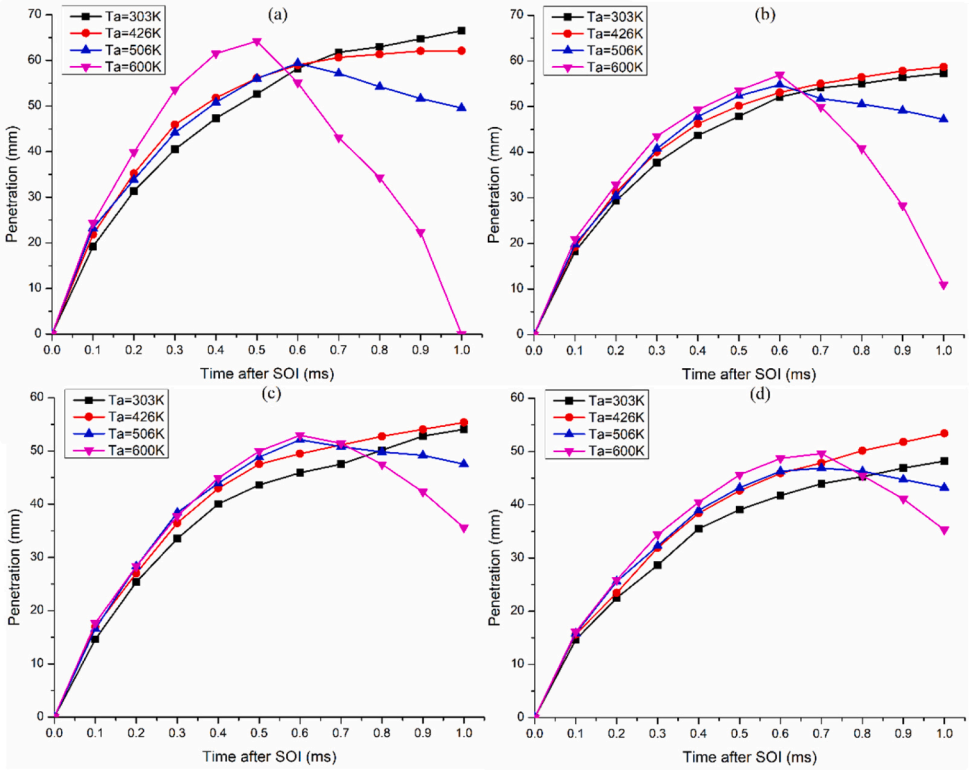

Fig. A6. Effect of T_a on spray penetration of DF at 1200 bar P_r and P_a of 10 bar (a), 20 bar (b), 30 bar (c) and 40 bar (d).

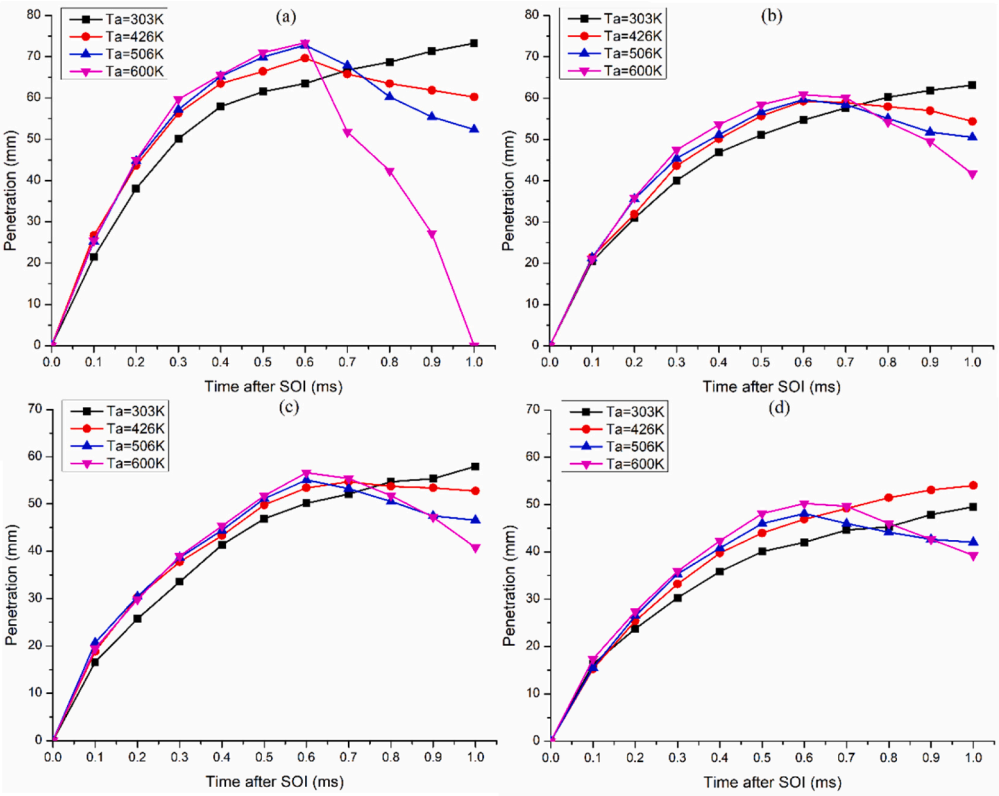

Fig. A7. Effect of T_a on spray penetration of DF at 1500 bar P_r and P_a of 10 bar (a), 20 bar (b), 30 bar (c) and 40 bar (d).

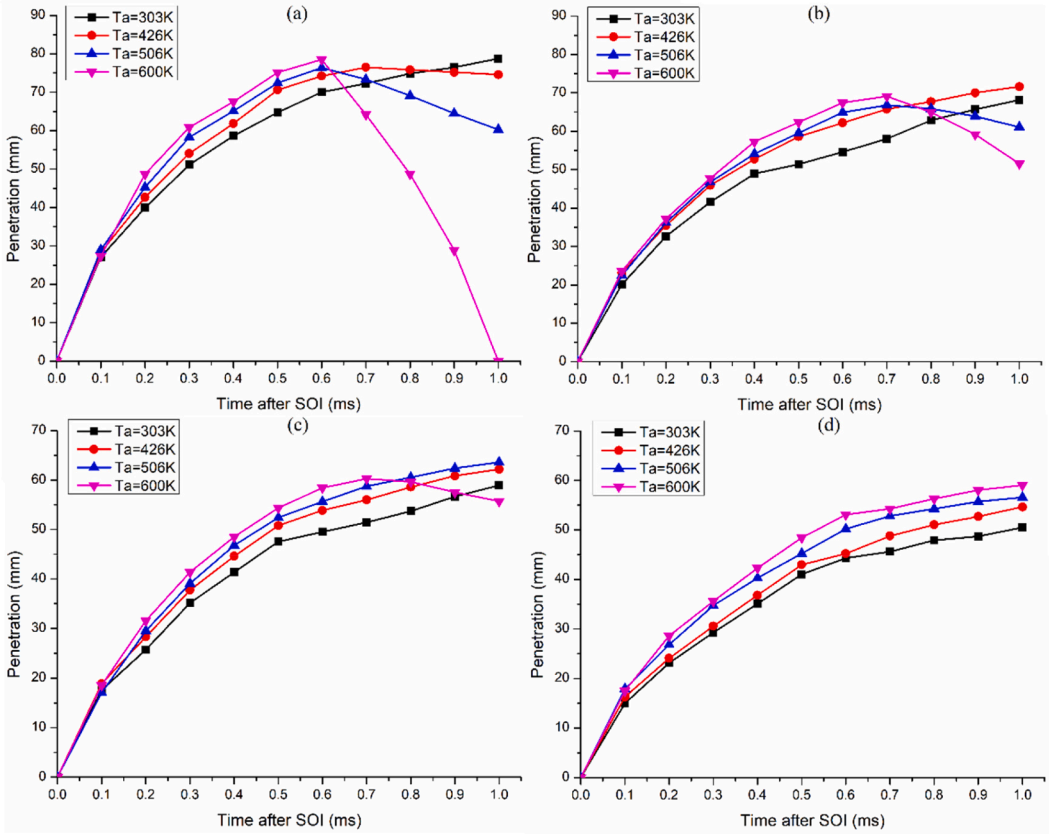

Fig. A8. Effect of T_a on spray penetration of DF at 1800 bar P_r and P_a of 10 bar (a), 20 bar (b), 30 bar (c) and 40 bar (d).

Table A1
Distillation values of GTL and diesel fuel [35].

Distillation (vol)	DF	GTL
10%	207.6	213.9
50%	278.2	269.3
90%	345.0	340.7

Table A2
Experimental conditions for DF spray.

Condition (Test order)	P_r (bar)	P_a (bar)	T_a (K)	Condition (Test order)	P_r (bar)	P_a (bar)	T_a (K)
1	900	10	303	33	1500	10	303
2	900	10	426	34	1500	10	426
3	900	10	506	35	1500	10	506
4	900	10	600	36	1500	10	600
5	900	20	303	37	1500	20	303
6	900	20	426	38	1500	20	426
7	900	20	506	39	1500	20	506
8	900	20	600	40	1500	20	600
9	900	30	303	41	1500	30	303
10	900	30	426	42	1500	30	426
11	900	30	506	43	1500	30	506
12	900	30	600	44	1500	30	600
13	900	40	303	45	1500	40	303
14	900	40	426	46	1500	40	426
15	900	40	506	47	1500	40	506
16	900	40	600	48	1500	40	600
17	1200	10	303	49	1800	10	303
18	1200	10	426	50	1800	10	426
19	1200	10	506	51	1800	10	506
20	1200	10	600	52	1800	10	600
21	1200	20	303	53	1800	20	303
22	1200	20	426	54	1800	20	426
23	1200	20	506	55	1800	20	506
24	1200	20	600	56	1800	20	600
25	1200	30	303	57	1800	30	303
26	1200	30	426	58	1800	30	426
27	1200	30	506	59	1800	30	506
28	1200	30	600	60	1800	30	600
29	1200	40	303	61	1800	40	303
30	1200	40	426	62	1800	40	426
31	1200	40	506	63	1800	40	506
32	1200	40	600	64	1800	40	600

References

[1] Allocca L, Mancaruso E, Montanaro A, Sequino L, Vaglieco BM. Evaluation of RME (rapeseed methyl ester) and mineral diesel fuels behaviour in quiescent vessel and EURO 5 engine. Energy 2014;77:783–90.
[2] COMMISSION REGULATION (EU) 2016/1718. In: (EU) CR, ed. 2016/1718. Commission Regulation (EU); 2016.
[3] Rho B-J, Kang S-J, Oh J-H, Lee S-G. Swirl effect on the spray characteristics of a twin-fluid jet. KSME International Journal 1998;12(5):899–906.
[4] Park SH, Youn IM, Lim Y, Lee CS. Influence of the mixture of gasoline and diesel fuels on droplet atomization, combustion, and exhaust emission characteristics in a compression ignition engine. Fuel Process Technol 2013;106:392–401.
[5] Heng HC, Idrus S. The future of gas to liquids as a gas monetisation option. J Nat Gas Chem 2004;13(2):63–70.
[6] Mancaruso E, Sequino L, Vaglieco BMJE. GTL (Gas To Liquid) and RME (Rapeseed Methyl Ester) combustion analysis in a transparent CI (compression ignition) engine by means of IR (infrared) digital imaging. Energy 2013;58:185–91.
[7] Wu T, Huang Z, Zhang W-G, Fang J-H, Yin Qi. Physical and chemical properties of GTL– diesel fuel blends and their effects on performance and emissions of a multicylinder DI compression ignition engine. Energy Fuels 2007;21(4):1908–14.
[8] Soltic P, Edenhauser D, Thurnheer T, Schreiber D, Sankowski A. Experimental investigation of mineral diesel fuel, GTL fuel, RME and neat soybean and rapeseed oil combustion in a heavy duty on-road engine with exhaust gas aftertreatment. Fuel 2009;88(1):1–8.
[9] Wood DA, Nwaoha C, Towler BF. Gas-to-liquids (GTL): A review of an industry offering several routes for monetizing natural gas. J Nat Gas Sci Eng 2012;9:196–208.
[10] Abu-Jrai A, Rodríguez-Fernández J, Tsolakis A, Megaritis A, Theinnoi K, Cracknell RF, et al. Performance, combustion and emissions of a diesel engine operated with reformed EGR. Comparison of diesel and GTL fuelling. Fuel 2009;88(6):1031–41.
[11] Hassaneen A, Munack A, Ruschel Y, Schroeder O, Krahl J. Fuel economy and emission characteristics of Gas-to-Liquid (GTL) and Rapeseed Methyl Ester (RME) as alternative fuels for diesel engines. Fuel 2012;97:125–30.
[12] Tira HS, Herreros JM, Tsolakis A, Wyszynski ML. Characteristics of LPG-diesel dual fuelled engine operated with rapeseed methyl ester and gas-to-liquid diesel fuels. Energy 2012;47(1):620–9.
[13] Kannaiyan K, Sadr R. Experimental investigation of spray characteristics of alternative aviation fuels. Energy Convers Manage 2014;88:1060–9.
[14] Gumus S, Ozcan H, Ozbey M, Topaloglu B. Aluminum oxide and copper oxide nanodiesel fuel properties and usage in a compression ignition engine. Fuel 2016;163:80–7.
[15] Saxena V, Kumar N, Saxena VK. A comprehensive review on combustion and stability aspects of metal nanoparticles and its additive effect on diesel and biodiesel fuelled CI engine. Renew Sustain Energy Rev 2017;70:563–88.
[16] Vairamuthu G, Sundarapandian S, Kailasanathan C, Thangagiri B. Experimental investigation on the effects of cerium oxide nanoparticle on calophyllum inophyllum (Punnai) biodiesel blended with diesel fuel in DI diesel engine modified by nozzle geometry. J Energy Inst 2016;89(4):668–82.
[17] Kumar S, Dinesha P, Rosen MA. Effect of injection pressure on the combustion, performance and emission characteristics of a biodiesel engine with cerium oxide nanoparticle additive. Energy 2019;185:1163–73.
[18] Aghbashlo M, Tabatabaei M, Khalife E, Najafi B, Mirsalim SM, Gharehghani A, et al. A novel emulsion fuel containing aqueous nano cerium oxide additive in diesel–biodiesel blends to improve diesel engines performance and reduce exhaust emissions: Part II–Exergetic analysis. Fuel 2017;205:262–71.
[19] Khalife E, Tabatabaei M, Najafi B, Mirsalim SM, Gharehghani A, Mohammadi P, et al. A novel emulsion fuel containing aqueous nano cerium oxide additive in diesel–biodiesel blends to improve diesel engines performance and reduce exhaust emissions: Part I-Experimental analysis. Fuel 2017;207:741–50.
[20] Soukht Saraee H, Taghavifar H, Jafarmadar S. Experimental and numerical consideration of the effect of CeO2 nanoparticles on diesel engine performance and exhaust emission with the aid of artificial neural network. Appl Therm Eng 2017;113:663–72.

[21] Mirzajanzadeh M, Tabatabaei M, Ardjmand M, Rashidi A, Ghobadian B, Barkhi M, et al. A novel soluble nano-catalysts in diesel–biodiesel fuel blends to improve diesel engines performance and reduce exhaust emissions. Fuel 2015;139:374–82.
[22] Najafi G. Diesel engine combustion characteristics using nano-particles in biodiesel-diesel blends. Fuel 2018;212:668–78.
[23] Heydari-Maleney K, Taghizadeh-Alisaraei A, Ghobadian B, Abbaszadeh-Mayvan A. Analyzing and evaluation of carbon nanotubes additives to diesohol-B2 fuels on performance and emission of diesel engines. Fuel 2017;196:110–23.
[24] Ooi JB, Ismail HM, Tan BT, Wang X. Effects of graphite oxide and single-walled carbon nanotubes as diesel additives on the performance, combustion, and emission characteristics of a light-duty diesel engine. Energy 2018;161:70–80.
[25] Malakkal L, Prasad A, Oladimeji D, Jossou E, Ranasinghe J, Szpunar B, et al. Atomistic and experimental study on thermal conductivity of bulk and porous cerium dioxide. 2019;9(1):1-14.
[26] Han Z, Fina AJPips. Thermal conductivity of carbon nanotubes and their polymer nanocomposites: A review. 2011;36(7):914-44.
[27] Janke I, Neto MAM, Barbosa Jr JR, Garzon NN, Hartmann RM, Oliveira Jr AJRP, SP, Brazil. Viscosity and thermal conductivity of soybean oil-diesel blends between 293 and 353 K. 2013:7.
[28] Das D, Nerella S, Kulkarni DJPs, technology. Thermal properties of petroleum and gas-to-liquid products. 2007;25(4):415-25.
[29] Zhang Z, Lu Y, Roskilly AP, Yu X, Wang Y, Smallbone A. Investigation of the macroscopic characteristics of Hydrotreated Vegetable Oil (HVO) spray using CFD method. Fuel 2019;237:28–39.
[30] Chen P-C, Wang W-C, Roberts WL, Fang T. Spray and atomization of diesel fuel and its alternatives from a single-hole injector using a common rail fuel injection system. Fuel 2013;103:850–61.
[31] Zhang Z, Lu Y, Wang Y, Yu X, Smallbone A, Dong C, et al. Comparative study of using multi-wall carbon nanotube and two different sizes of cerium oxide nanopowders as fuel additives under various diesel engine conditions. Fuel 2019; 256:115904. https://doi.org/10.1016/j.fuel.2019.115904.
[32] Ma Y, Huang S, Huang R, Zhang Yu, Xu S. Spray and evaporation characteristics of n-pentanol–diesel blends in a constant volume chamber. Energy Convers Manage 2016;130:240–51.
[33] Mohan B, Yang W, Tay KL, Yu W. Experimental study of spray characteristics of biodiesel derived from waste cooking oil. Energy Convers Manage 2014;88: 622–32.
[34] Legg J, Narvaez A, McDonell V. Performance of algae-derived renewable diesel in a twin-fluid airblast atomizer. *Proceedings of the 12th triennial international conference on liquid atomization and spray systems, Heidelberg, Germany Google Scholar*. 2012: 56-65.
[35] Soriano JA, Garcia-Contreras R, Leiva-Candia D, Soto FJE, fuels. Influence on performance and emissions of an automotive diesel engine fueled with biodiesel and paraffinic fuels: GTL and biojet fuel farnesane. 2018;32(4):5125-33.